Available online at www.sciencedirect.com
ScienceDirect
Journal of Power Sources 160 (2006) 316–325
JOURNAL OF POWER SOURCES
www.elsevier.com/locate/jpowsour

Power and temperature control of fluctuating biomass gas fueled solid oxide fuel cell and micro gas turbine hybrid system

T. Kaneko, J. Brouwer*, G.S. Samuelsen

National Fuel Cell Research Center, 323 Engineering Laboratory Facility, University of California, Irvine, CA 92697-3550, USA

Received 3 December 2005; received in revised form 5 January 2006; accepted 11 January 2006
Available online 3 March 2006

Abstract

This paper addresses how the power and temperature are controlled in a biomass gas fueled solid oxide fuel cell (SOFC) and micro gas turbine (MGT) hybrid system. A SOFC and MGT dynamic model are developed and used to simulate the hybrid system performance operating on biomass gas. The transient behavior of both the SOFC and MGT are discussed in detail.

An unstable power output is observed when the system is fed biomass gas. This instability is due to the fluctuation of gas composition in the fuel. A specially designed fuel controller succeeded not only in allowing the hybrid system to follow a step change of power demand from 32 to 35 kW, but also stably maintained the system power output at 35 kW. In addition to power control, fuel cell temperature is controlled by introduction and use of a bypass valve around the recuperator. By releasing excess heat to the exhaust, the bypass valve provided the control means to avoid the self-exciting behavior of system temperature and stabilized the temperature of SOFC at 850 °C.

Keywords: Hybrid system; Control; Solid oxide fuel cell; Micro gas turbine; Biomass gas

1. Introduction

Small-sized distributed generation systems are known to potentially produce electricity to reduce fuel consumption and carbon dioxide (CO_2) emissions that contribute to global climate change. A few micro turbine generator systems are commercially produced today. However, electrical efficiency for these types of generators is lower than 30% [1], requiring a substantial use of co-generated heat to reduce fuel consumption and CO_2 emissions. On the other hand, society consumes two thirds of its energy requirements in the form of electricity [2]. From that point of view, improvement in electrical efficiency of small sized distributed generators is a significant technological requirement.

One promising way to improve electrical efficiency of a micro gas turbine generator is to build it into a hybrid system with solid oxide fuel cell (SOFC). Various designs have been proposed that essentially use the waste heat of the SOFC to power the gas turbine system. In general, hybrid systems consist of a high temperature fuel cell (e.g., SOFC) integrated into a cycle with a micro gas turbine (MGT). This type of hybrid system has been proven to have electrical efficiency of up to 53% at 200 kW output [3], and is considered to have potential electrical efficiencies that are higher than 60% [4–6]. To further study and understand the SOFC-MGT hybrid system, both static [7–9] and dynamic [10–13] performance analyses have been conducted recently.

In addition to the distributed generation strategy, the importance of utilizing renewable energy, such as solar, wind, and biomass energy, is required to reduce both the consumption of fossil resources and the emission of CO_2. From this point of view, an integrated energy strategy for the future is to develop a small-sized distributed generation system coupled with renewable fuel. This strategy is also important for the efficient use of renewable resources, which are often dispersed over a wide area.

In this paper, a control strategy for a small sized SOFC-MGT hybrid system fueled by biomass gas is discussed. The system has to rapidly follow changes in power demand while maintaining appropriate system temperatures. In addition, since the system is fueled by biomass gas, it has to be robust to changes of

* Corresponding author. Tel.: +1 949 824 7302; fax: +1 949 824 7423.
E-mail addresses: tk@apep.uci.edu (T. Kaneko), jb@apep.uci.edu (J. Brouwer), gss@apep.uci.edu (G.S. Samuelsen).

0378-7753/$ – see front matter © 2006 Elsevier B.V. All rights reserved.
doi:10.1016/j.jpowsour.2006.01.044

the gas composition of fuel, which changes are often caused in the decomposition process of biomass resources (e.g., anaerobic digestion). Both to obtain insights into system behavior and to provide a reliable design support tool, the dynamic simulation and control strategies for biomass fueled SOFC-MGT hybrid systems are highly desired.

2. Hybrid system model description

The current model is developed to study the potential performance of an existing two-shaft 5 kW MGT system that is being tested at the University of Tokyo, Japan. After initial stand-alone testing, this MGT will be integrated into a hybrid solid oxide fuel cell gas turbine system. The hybrid system described in this paper (see Fig. 1) produces 35 kW at rated output and consists of a compressor, recuperator, SOFC, combustor, two turbines, and a bypass valve. The SOFC is used as a topping cycle, that is, it operates under the pressurized conditions between the compressor and first turbine of the MGT. One turbine is directly connected by a shaft to drive the compressor and the other turbine is connected to an electric generator. The biomass gas fueled is pressurized and preheated before entering the SOFC to avoid excess cooling and thermal stress in the fuel cell stack. A bypass valve is for controlling the portion of exhaust gas flow goes into recuperator. Fig. 1 shows the entire system schematic.

A dynamic SOFC model and a MGT model are developed in a Matlab/Simulink^{TM} environment, considering mass balance, momentum balance, energy balance, chemical and electrochemical reactions, and electrochemical losses.

2.1. SOFC model

2.1.1. Operating cell voltage

The operating cell voltage (V) is theoretically determined through calculation of the Nernst voltage, activation overpotential, concentration overpotential, and ohmic overpotential. The effect of carbon monoxide on electro-chemical potential is neglected since water-gas shift chemistry is much faster than CO electro-oxidation in the high temperature fuel cell of interest. Studies have found that as much as 98% of the CO reacts via this route (shift reaction followed by H_2 electro-oxidation) in an SOFC [14]. Note that pressure in the anode and cathode compartments are assumed to be the same.

Operating cell voltage

$$V = E - V_{\text{act}} - V_{\text{conc}} - V_{\text{ohm}} \tag{1}$$

Nernst potential

$$E = E^0 + \frac{R_u T}{2F} \ln\left(\frac{\chi_{H_2}\chi_{O_2}^{1/2}}{\chi_{H_2O}}\left(\frac{P_C}{P_0}\right)^{1/2}\right) \tag{2}$$

Activation, concentration, and ohmic overpotentials

$$V_{\text{act}} = \frac{R_u T}{2\alpha F} \ln\left(\frac{i}{i_{\text{ex}}}\right) \tag{3}$$

$$V_{\text{conc}} = \frac{R_u T}{2F} \ln\left(1 - \frac{i}{i_l}\right) \tag{4}$$

$$V_{\text{ohm}} = i\,R \tag{5}$$

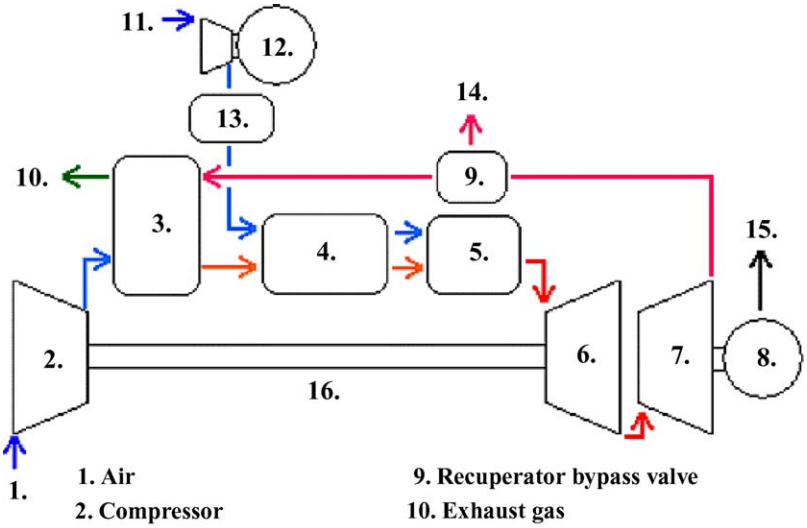

1. Air
2. Compressor
3. Recuperator
4. SOFC
5. Combustor
6. High-pressure turbine
7. Power turbine
8. Generator
9. Recuperator bypass valve
10. Exhaust gas
11. Biomass gas
12. Fuel compressor
13. Fuel preheater
14. Bypassed exhaust gas
15. Electricity
16. Shaft

Fig. 1. Schematic of SOFC SOFC-MGT hybrid system. This figure presents a schematic of the system described in the paper. The SOFC is a topping cycle between the compressor and high-pressure turbine of a two-shaft micro gas turbine. The system also contains a fuel compressor, fuel preheater, and exhaust gas bypass valve.

In this paper, the current production of the fuel cell is determined by solution of Eqs. (1)–(5) by maintaining a fuel cell voltage of 0.7 V. This is realistic since we assume that the fuel cell is connected to an inverter with feedback control on the fuel cell voltage. The power electronics of the inverter are very fast allowing for quick changes in the amount of current drawn from the fuel cell to maintain fuel cell voltage at 0.7 V.

2.1.2. Heat transfer in the SOFC

Temperatures in all cell components have to be calculated to consider heat transfer by conduction, convection, and radiation. Temperatures that are essential to accurately determine include the temperature of the reformer, fuel separator, anode, electrolyte, cathode, and oxidant separator. An internal reformer is included in the current fuel cell design between the fuel separator and oxidant separator. It is assumed that no mass or heat is transferred to the environment. Fig. 2 shows how heat transfer occurs between each component and the gas streams. The dynamic equations that govern the heat transfer processes include heat conduction between solids, heat convection between flowing gases and solid surfaces, and heat radiation between solid surfaces in each cell component shown in Fig. 2. These equations have been described in detail elsewhere [12]. Note that there is heat generation in the cell due to the voltage losses and negative heat generation in the reformer due to endothermic reformation reactions.

2.1.3. Chemical kinetics

There are three main sets of chemical kinetics that one should consider for the current hybrid fuel cell system. These chemical kinetics are those associated with anode reactions, cathode reactions, and reformation reactions. Hydrogen is assumed to be the only electrochemically active species in the anode compartment and oxygen is the only electrochemically active species in the cathode compartment. However, there are three chemical reactions considered in the reformation chemistry. These reactions are the methane reformation reaction, water-gas shift reaction, and overall reformation reaction. Note that these reactions can also occur within the anode compartment of the fuel cell. In the following equations, X and R vectors are used to represent the mole fraction and rate (respectively) of 7 individual species, which are methane, carbon monoxide, carbon dioxide, hydrogen, water, nitrogen, and oxygen. Also, note that I is current, not current density. Each rate of chemical reaction and chemical equilibrium coefficient is based on previous research (Xu and Froment [15,16]).

Anode reaction

$$H_2 + O^{2-} \xrightarrow{\text{anode}} H_2O + 2e^- \tag{6}$$

$$\vec{R}_a = \left[0 \quad 0 \quad 0 \quad \left(-\frac{I}{2F}\right) \quad \left(+\frac{I}{2F}\right) \quad 0 \quad 0\right] \tag{7}$$

$$I = i\,A_{cell} \tag{8}$$

$$\dot{N}\frac{d\vec{X}}{dt} = \left(\dot{N}\vec{X}\right)_{in} - \left(\dot{N}\vec{X}\right)_{out} + \vec{R}_a + \vec{R}_{ref-a} \tag{9}$$

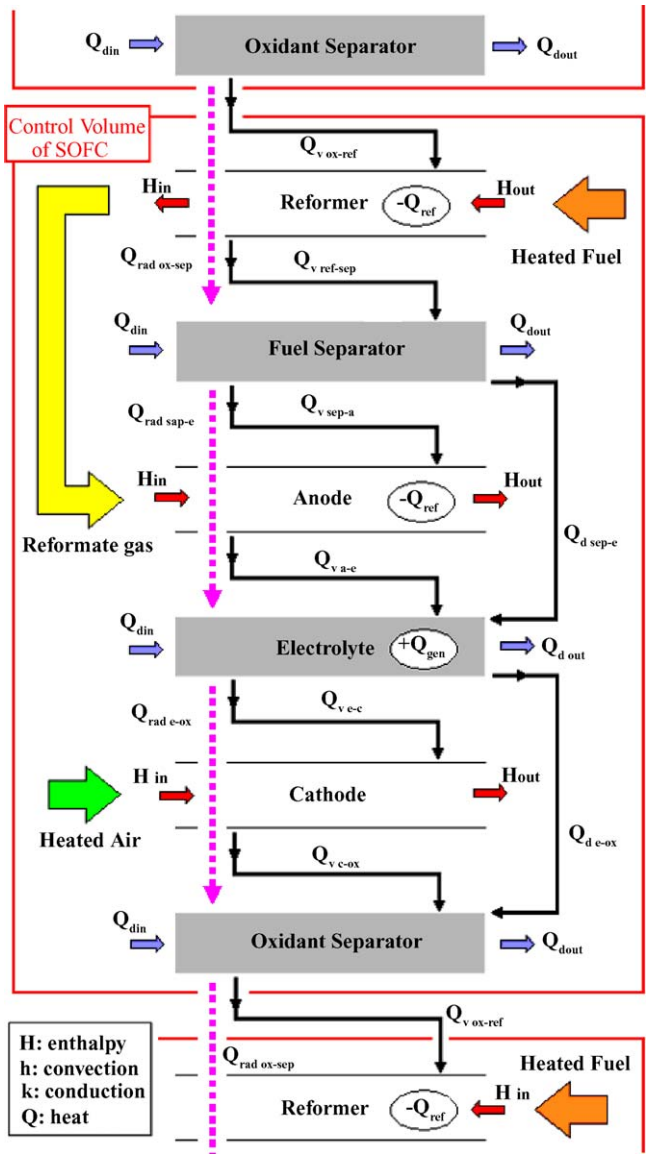

Fig. 2. Schematic of heat transfer in each component. This figure shows the major components together with the energy and mass flows of the SOFC stack. The indirect internal reformation SOFC contains a reformer section, anode, electrolyte, cathode, and gas separators. Red box indicates unit control volume. (For interpretation of the references to colour in this figure caption, the reader is referred to the web version of the article.)

Cathode reaction

$$\tfrac{1}{2}O_2 + 2e^- \xrightarrow{\text{cathode}} O^{2-} \tag{10}$$

$$\vec{R}_c = \left[0 \quad 0 \quad 0 \quad 0 \quad 0 \quad 0 \quad \left(-\frac{I}{4F}\right)\right] \tag{11}$$

$$\dot{N}\frac{d\vec{X}}{dt} = \left(\dot{N}\vec{X}\right)_{in} - \left(\dot{N}\vec{X}\right)_{out} + \vec{R}_c \tag{12}$$

Reforming reactions [15,16]

$$CH_4 + H_2O \xrightarrow{r_1} CO + 3H_2 - \Delta\bar{h}_1 \tag{13}$$

$$CO + H_2O \xrightarrow{r_2} CO_2 + H_2 + \Delta\bar{h}_2 \tag{14}$$

$$CH_4 + 2H_2O \xrightarrow{r_3} CO_2 + 4H_2 - \Delta\bar{h}_3 \tag{15}$$

$$\vec{R}_{\text{ref}} = \begin{bmatrix} r_{CH_4} & r_{CO} & r_{CO_2} & r_{H_2} & r_{H_2O} & r_{N_2} & r_{O_2} \end{bmatrix} = \begin{bmatrix} -r_1 - r_3 \\ r_1 - r_2 \\ r_2 + r_3 \\ 3r_1 + r_2 + 4r_3 \\ -r_1 - r_2 - 2r_3 \\ 0 \\ 0 \end{bmatrix}^T \tag{16}$$

$$\dot{N}\frac{d\vec{X}}{dt} = \left(\dot{N}\vec{X}\right)_{\text{in}} - \left(\dot{N}\vec{X}\right)_{\text{out}} + \vec{R}_{\text{ref}} \tag{17}$$

All the equations governing heat transfer and chemical reactions are solved simultaneously to calculate the temperature and gas concentrations for Eqs. (1)–(5).

2.2. MGT model

The MGT model consists of a compressor, fuel compressor, recuperator, combustor, two turbines, and a shaft model. The high-pressure turbine is connected directly to the compressor by the shaft. Electrical power from the MGT is derived from an electric generator connected to the power turbine. No mass or heat losses to the environment are considered.

Both enthalpy and mass flow rate of the working fluid at each state point are required to calculate the available work from the turbines and required work of the compressor. For enthalpy, thermodynamic relation and efficiency equations in both the compressor and turbine are solved to determine temperatures from which enthalpy is determined for a known composition. The isentropic efficiencies of the compressor and turbine are fixed to 0.75 and 0.85, respectively. This compressor efficiency is chosen because it well represents measured compressor performance at the University of Tokyo over a range of operation. The turbine efficiency is selected as the goal of current research underway to improve small turbine performance that is ongoing at the University of Tokyo. Note that in the turbine model, the specific heat ratio cannot be assumed as a fixed number because its dependency to the temperature greatly increases at high temperatures. A compressor map is used to calculate air mass flow rate from rotor speed and pressure ratio. The design point parameters for the system and compressor map, which are constant during the simulation, are shown in Table 1 and Fig. 3, respectively. The design rotational speed of each turbine is set to 120,000 rpm since it is the desire of the current research project to use the same turbine as the high-pressure turbine and power turbine to reduce system cost.

In the combustor model, perfect combustion efficiency under adiabatic conditions is assumed. Since turbine inlet temperature never exceeds 2000 K in this research, it is sufficient to calculate flame temperature from a simple energy balance.

Table 1
Hybrid fuel cell micro gas turbine design model parameters

SOFC		
Number of cells		1200
A_{cell}		100 cm^2
E^0		$(245{,}863 - 51.135T - 2.136 \times 10^{-3}\,T^2)/2F$
i_{ex}		500
α		0.5
i_{l}		4000
R		$-4.167 \times 10^{-6}(T-273) + 5.833 \times 10^{-3}$
MGT		
Compressor	T_{des}	298 K
	ω_{des}	120,000 rpm
High-pressure turbine	m_{des}	0.043 kg s^{-1}
	T_{des}	1173 K
	P_{des}	200 kPa
	ω_{des}	120,000 rpm
Power turbine	m_{des}	0.043 kg s^{-1}
	T_{des}	1173 K
	P_{des}	160 kPa
	ω_{des}	120,000 rpm
Shaft	J	6.6×10^{-5} kg m^2

This table shows the values of each of the major parameters used in the simulation.

In the recuperator model, the upper stream (compressor discharge air) is heated by convection heat transfer from the separation plate, which is correspondingly heated by convection heat transfer from the lower stream (turbine exhaust). Conduction heat transfer inside the stream separation plate along the streamwise direction is also considered, while heat transfer along the thickness of the plate is not taken into account because the plate is assumed to be thin.

The rotational speed of the shaft, which is the same as that of the compressor and high-pressure turbine, is determined by the sum of torques method as follows. Since no load is added on the shaft, and no bearing friction of the shaft is considered, there is no loss term in the momentum equation for the shaft.

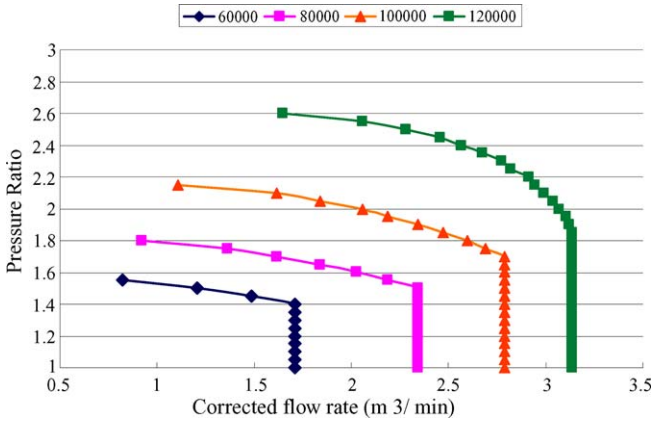

Fig. 3. Compressor map. This figure shows the performance map of the compressor. The different lines correspond to different rotational speeds. Vertical lines imply choking of compressor.

Compressor

$$\frac{\omega}{\sqrt{T}} = \frac{\omega_{\mathrm{des}}}{\sqrt{T_{\mathrm{des}}}} = \mathrm{Const.} \tag{18}$$

$$T_{02} = T_{01}\left(1 + \frac{1}{\eta_{\mathrm{c}}}\left(\left(\frac{P_{02}}{P_{01}}\right)^{\gamma-1/\gamma} - 1\right)\right) \tag{19}$$

$$\dot{W}_{\mathrm{comp}} = -\dot{m}\int_{T_{01}}^{T_{02}} C_{\mathrm{p}}dT \tag{20}$$

Fuel compressor

$$\dot{W}_{\mathrm{comp,f}} = -\dot{m}_{\mathrm{f}}\int_{T_{01}}^{T_{02}} C_{\mathrm{p,f}}\,\mathrm{d}T \tag{21}$$

Recuperator

$$\frac{1}{2}\xi_{\mathrm{recup}}\,u_{\mathrm{up}}^2 = \frac{1}{\rho_{\mathrm{up}}}(P_{\mathrm{in}} - P_{\mathrm{out}})_{\mathrm{up}} \tag{22}$$

$$\frac{\mathrm{d}}{\mathrm{d}t}\left(C_{\mathrm{up}}\bar{C}_{\mathrm{p}}T_{\mathrm{up}}\right) = \left(\dot{N}\bar{h}\right)_{\mathrm{in}} - \left(\dot{N}\bar{h}\right)_{\mathrm{out}} - \dot{Q}_{\mathrm{v,\,up\text{-}plate}} \tag{23}$$

$$\frac{\mathrm{d}}{\mathrm{d}t}(m_{\mathrm{plate}}C_{\mathrm{p,\,plate}}T_{\mathrm{plate}}) = \dot{Q}_{\mathrm{d,\,in}} - \dot{Q}_{\mathrm{d,\,out}} + \dot{Q}_{\mathrm{v,\,up\text{-}plate}} - \dot{Q}_{\mathrm{v,\,plate\text{-}down}} \tag{24}$$

$$\frac{1}{2}\,\xi_{\mathrm{recup}}\,u_{\mathrm{down}}^2 = \frac{1}{\rho_{\mathrm{down}}}(P_{\mathrm{in}} - P_{\mathrm{out}})_{\mathrm{down}} \tag{25}$$

$$\frac{\mathrm{d}}{\mathrm{d}t}(C_{\mathrm{down}}\bar{C}_{\mathrm{p}}T_{\mathrm{down}}) = (\dot{N}\bar{h})_{\mathrm{in}} - (\dot{N}\bar{h})_{\mathrm{out}} + \dot{Q}_{\mathrm{v,\,plate\text{-}down}} \tag{26}$$

Combustor

$$0 = \sum_{\mathrm{prod}}\dot{N}\left(\bar{h}_{\mathrm{f}}^0 + \int_{298}^{T}\bar{C}_{\mathrm{p}}\,\mathrm{d}T\right) - \sum_{\mathrm{react}}\dot{N}\left(\bar{h}_{\mathrm{f}}^0 + \int_{298}^{T}\bar{C}_{\mathrm{p}}\,\mathrm{d}T\right) \tag{27}$$

$$\mathrm{CH_4} + 2(\mathrm{O_2} + 3.76\mathrm{N_2}) \xrightarrow{r_1'} \mathrm{CO_2} + 2\mathrm{H_2O} + 7.52\mathrm{N_2} \tag{28}$$

$$\mathrm{CO} + \tfrac{1}{2}(\mathrm{O_2} + 3.76\mathrm{N_2}) \xrightarrow{r_2'} \mathrm{CO_2} + 1.88\mathrm{N_2} \tag{29}$$

$$\mathrm{H_2} + \tfrac{1}{2}(\mathrm{O_2} + 3.76\mathrm{N_2}) \xrightarrow{r_3'} \mathrm{H_2O} + 1.88\mathrm{N_2} \tag{30}$$

$$\vec{R}_{\mathrm{comb}} = \begin{bmatrix} -r_1' \\ -r_2' \\ r_1' + r_2' \\ -r_3' \\ 2r_1' + r_3' \\ 0 \\ -2r_1' - \frac{1}{2}r_2' - \frac{1}{2}r_3' \end{bmatrix}^T \tag{31}$$

$$\frac{1}{2}\,\xi_{\mathrm{comb}}\,u_{\mathrm{comb}}^2 = \frac{1}{\rho_{\mathrm{comb}}}(P_{\mathrm{in}} - P_{\mathrm{out}})_{\mathrm{comb}} \tag{32}$$

$$\frac{\mathrm{d}}{\mathrm{d}t}(C_{\mathrm{gas}}\bar{C}_{\mathrm{p}}T_{\mathrm{gas}}) = (\dot{N}\bar{h})_{\mathrm{in}} - (\dot{N}\bar{h})_{\mathrm{out}} - \dot{Q}_{\mathrm{v,\,gas\text{-}comb}} \tag{33}$$

Table 2
Predicted performance of the system at design conditions, including SOFC temperature control via recuperator bypass flow manipulation

Compressor out T (K)	395
Recuperator out T (K)	897
Cathode out T (K)	1119
Anode out T (K)	1117
Combustor out T (K)	1350
High-pressure turbine out T (K)	1289
Power turbine out T (K)	1195
Compressor exit P (kPa)	218
Air flow rate (kg s^{-1})	0.037
U_{f}	0.83
U_{air}	0.43
Current density (mA cm^{-2})	372
Fuel cell power output (kW)	297
Gas turbine power output (kW)	5.3
Total power output (kW)	35
Fuel	33.3% CH_4; 66.7% H_2O

This table shows the performance of the system at design point operation.

$$\frac{\mathrm{d}}{\mathrm{d}t}(m_{\mathrm{comb}}C_{\mathrm{p,\,comb}}T_{\mathrm{comb}}) = \dot{Q}_{\mathrm{v,\,gas\text{-}comb}} \tag{34}$$

Turbine

$$\frac{\dot{m}\sqrt{T}}{P} = \frac{\dot{m}_{\mathrm{des}}\sqrt{T_{\mathrm{des}}}}{P_{\mathrm{des}}} = \mathrm{Const.} \tag{35}$$

$$\frac{\omega}{\sqrt{T}} = \frac{\omega_{\mathrm{des}}}{\sqrt{T_{\mathrm{des}}}} = \mathrm{Const.} \tag{36}$$

$$T_{04} = T_{01}\left(1 + \eta_{\mathrm{t}}\left(\left(\frac{P_{04\mathrm{s}}}{P_{03}}\right)^{\gamma-1/\gamma} - 1\right)\right) \tag{37}$$

$$\gamma = \frac{C_{\mathrm{p}}}{C_{\mathrm{p}} - R_{\mathrm{u}}} \tag{38}$$

$$\dot{W}_{\mathrm{turb}} = \dot{m}\int_{T_{04}}^{T_{03}} C_{\mathrm{p}}\,\mathrm{d}T \tag{39}$$

Shaft

$$J\dot{\omega} = \frac{1}{\omega}(\dot{W}_{\mathrm{comp}} + \dot{W}_{\mathrm{turb}}) \tag{40}$$

3. Results and discussion

3.1. Predicted performance of SOFC-MGT hybrid system under design conditions

Table 2 shows the predicted performance of SOFC-MGT hybrid system for design conditions of a constant natural gas flow and composition. Total system power output is 35 kW, about 85% of that is from the SOFC and 15% is from MGT. Total system efficiency is 56.3%, which is quite high for this size of machinery for distributed generation. These predictions include DC–AC inverter efficiency (95%), electric generator efficiency (98%), fuel compression work, and the power to the fuel preheater to preheat the fuel mixture from 298 to 900 K before it is fed into SOFC. This power for preheating the fuel mixture is the

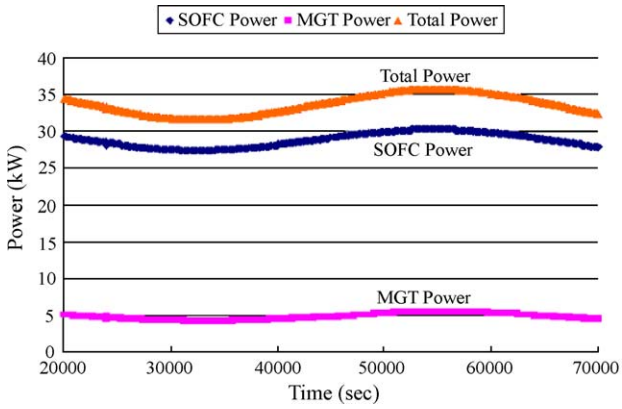

Fig. 4. System behavior in biomass gas. This graph presents the hybrid system output while operating on the fluctuating biomass fuel. Both the power of fuel cell and that of the micro turbine fluctuates significantly.

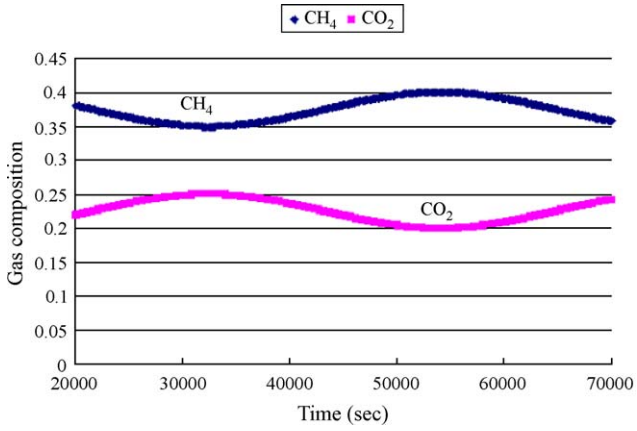

Fig. 5. Biomass fuel component fluctuation. This figure shows how the concentrations of biomass gas change versus time. The composition fluctuations are in a cycle of 12 h (43,200 s) to simulate a potentially reasonable diurnal cycle. The gas is kept humidified at 40%, while the total concentration of methane and carbon dioxide is kept equal to 60%.

largest parasitic loss among these at approximately 3.5 kW or 10% of system output. The fuel used for the design case (not the renewable fuel case) is a mixture of 33.3% methane and 66.7% water (i.e., steam-to-carbon ratio (S/C) is 2). In this case, the fuel must contain steam since the system does not have anode gas recirculation, which is a popular way to add both thermal enthalpy and steam to the fuel. To avoid overheating the fuel cell the system contains a recuperator bypass that was set to 50% open.

3.2. System performances in biomass gas fueling

Fig. 4 shows the predicted system performance behavior in the case when the system is fed biomass gas instead of the methane used for the design case. The gas composition of the biomass gas is provided in Table 3 and its compositional fluctuation is shown in Fig. 5. The maximum ratio of methane to carbon dioxide is chosen as 2, which is a typical number for biomass gas (e.g., anaerobic digester gas). The amount of steam in the fuel gas is 40% because a considerable amount of reformation reaction takes place in the anode where a lot of steam is available. The frequency of fluctuation is chosen to be 43,200 s, which is 12 h, to represent a diurnal fluctuation of biomass gas components like that, which could occur with an anaerobic digester.

Table 3
Biomass gas concentration

CH_4	0.35–0.4
CO	0
CO_2	0.25–0.2
H_2	0
H_2O	0.4
N_2	0
O_2	0
Total	1

This table shows the concentration of each gas species in the fluctuating biomass gas discussed in this paper. The composition roughly corresponds to digester gas that is humidified to 40% to facilitate reformation in the fuel cell. Methane and carbon dioxide concentrations vary between 35 and 40% and between 20 and 25%, respectively.

Although the molar flow rate of the gas is constant, power output from both the SOFC and MGT fluctuate due to the change of gas concentrations in biomass gas. It is observed that the system power changes nearly 13% even though the fuel component fluctuation is only 5% on an energy basis.

The power output from the SOFC and MGT is directly related to the fluctuation of the methane concentration and almost no delay is observed between the gas constituent change and the power fluctuation. As for the SOFC, this nearly instantaneous response is due to the rapid change in anode hydrogen concentration, which is produced by rapid methane reformation and water gas shift chemistry affecting the Nernst potential. Since the voltage of this SOFC cell is fixed to 0.7 V by feedback control in the power electronics, a higher concentration of methane leads to higher current density increasing the power output from the SOFC. This is also the reason that the SOFC has a relatively large amplitude power fluctuation compared to that of the MGT. Since Nernst potential is quite sensitive to the hydrogen concentration, even a small change in fuel composition can lead to a large change in current density.

As for the MGT, on the other hand, its amplitude of power fluctuation is relatively small. This is because the MGT runs only on the unspent fuel and waste heat of the SOFC, which does not change as significantly with gas composition.

3.3. Controlling performance in biomass gas

A system power controller is designed and implemented in the system model. The controller uses a standard proportional, integral, differential (PID) strategy to manipulate fuel flow rate to maintain (control) the power output of the system. Fig. 6 shows the controlled power output of the system. The controller manipulates the biomass fuel flow rate whenever it detects a difference between power demand and the system output. Fig. 6 shows that the system power output with the PID controller not only well follows a step change of power demand from 32 to 35 kW, but also well maintains power even when fueled by a fluctuating biomass gas. The fluctuation in biomass gas com-

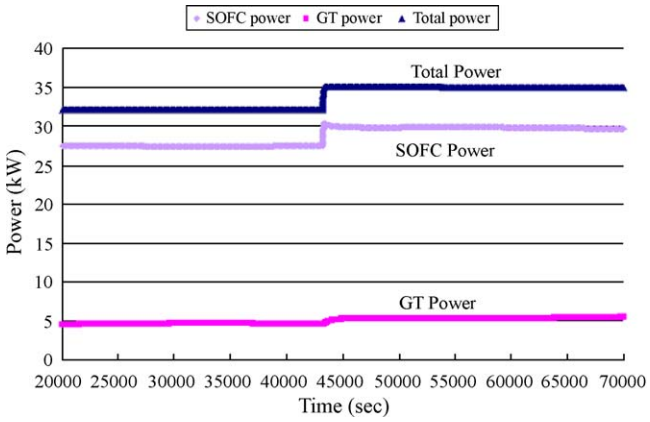

Fig. 6. Controlled power output in biomass gas operation. This is the system performance on fluctuating biomass gas after introducing power output control and temperature control. Power fluctuation due to the concentration fluctuation of biomass gas is no longer present. Note that the total power output quickly responds to the step change of power demand that occurs at 43,000 s.

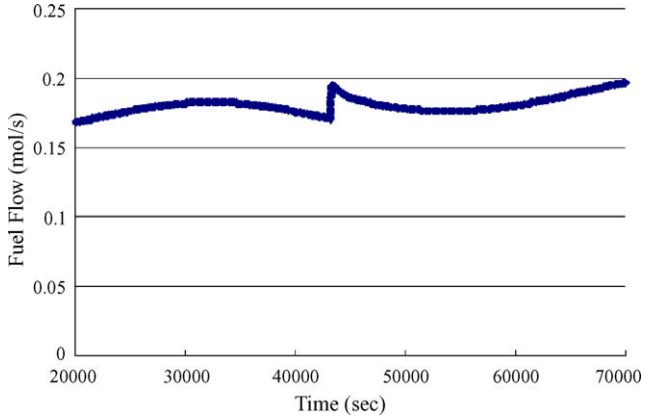

Fig. 7. Controlled biomass fuel flow rate. This is the graph showing how the fuel flow rate was manipuated by the installed controller. It shows that controller is trying to compensate for both the power fluctuation in the input fuel stream and the step change of power demand.

position used here is the same as that described in the previous section.

The transient response time of the system to the step change of total power demand is about 200 s. This is possible because the MGT responds relatively quickly to the change in power demand while the SOFC takes thousands of seconds to reach a new steady state power output level.

There are two overall mechanisms that contribute to the transient response of the SOFC power to the step change in load demand. The first response characteristic is the steep increase in power at the moment of the step change. In the moment of fuel flow increase, the Nernst potential jumps up due to rapid response of the chemical kinetics to produce a higher concentration of hydrogen in the anode compartment. This leads to higher current density (under the fixed voltage constraint), which means higher power output. In the second transient characteristic, however, hydrogen concentration starts to decrease because of the increased fuel consumption rate caused by the increased current density (and power production). The higher the current density becomes, the more hydrogen is consumed leading to a slow decrease in the Nernst potential. The slow decrease of Nernst potential leads to a slow decrease in current density and power output. After these two stages of transient response, power output from SOFC reaches a new steady state.

Typically, the above transients in fuel cell electrochemical performance consequently affect the temperature of the fuel cell (increased current production produces more heat). Since the SOFC comprises a large thermal mass, the temperature of the fuel cell would typically change with a long transient response time. This temperature transient would subsequently affect the long-term electrochemical performance of the fuel cell through Eqs. (2)–(4). However, this third transient stage is not present in Fig. 6. This is because the cell temperature of the current simulation case is maintained at 1123 K by use of a fuel cell temperature controller. This controller can bypass various amounts of exhaust flow around the recuperator to change the SOFC inlet air temperature. Under dynamic operating conditions, control of the hybrid system requires dynamic temperature control via variable exhaust bypass, as will be shown in Section 3.4.

The total power output is well maintained even though a slight power change is observed from both the SOFC and MGT during the final steady state operation due to the fluctuation of fuel composition. However, these power fluctuations are out of phase such that the sum of SOFC and MGT power is constant. When the SOFC provides more power, the amount of fuel in the anode off-gas is reduced resulting in lower combustor temperature and power output from MGT. This balance naturally occurs with the system power controller design of this study. Since the customer most desires good stabilization of total power output, this controlled system can be said to be robust to the biomass fuel composition fluctuation.

Fig. 7 shows the controlled fuel flow rate of biomass gas. The sudden change in fuel flow rate is in response to the step change of the power demand. The periodic (wavy) change in fuel flow rate of Fig. 7 is required by the controller to make up for the power fluctuations caused by the fluctuating biomass gas composition.

Fig. 8 shows the change of system efficiency when operating on fluctuating biomass fuel. Here the system efficiency is determined as the net power output divided by the total energy input. The net power output is the sum of power output from SOFC and MGT. The total energy input is the sum of biomass gas component lower heating values (LHV), including the effects of composition fluctuations, power used for fuel compression, and the heat input to the fuel preheater. The resulting hybrid system efficiency is between 55 and 58%. Fig. 8 also shows that the efficiency remains high even though the gas composition fluctuates. The reason for this is that both the total energy input by biomass gas and total power output of the system are almost kept constant by the respective controllers introduced into the system model. Since the system controls the fuel flow rate, the change of energy input to the system is small even though the fuel composition varies.

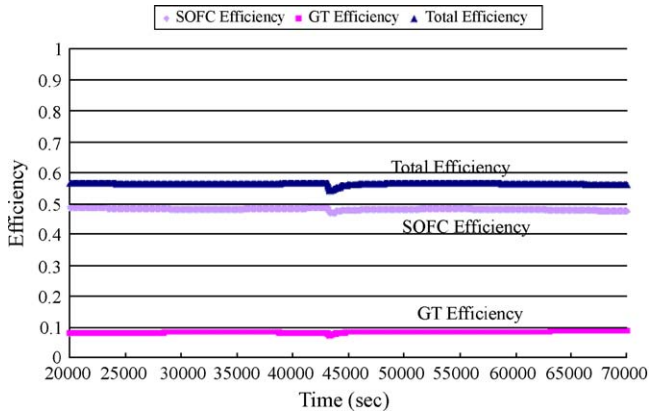

Fig. 8. System efficiencies. This graph shows how the efficiency varied when the power is controlled while operating on a fluctuating biomass fuel. There are only minor fluctuations due to the concentration change of the fuel, but, small decreases in efficiency are observed in the vicinity of the load step change.

Fig. 8 also shows the change of the efficiency of both the SOFC and MGT. Here each efficiency is determined as the power output from each component over the total energy input to the system. Because of this definition, the SOFC efficiency does not include fuel utilization and shows a relatively high efficiency. From Figs. 6 and 8, one can determine that the contribution of the MGT to the system power and efficiency is 14–16%.

Fig. 9 shows air and fuel utilization in the SOFC, which are between 44–48 and 81–83%, respectively. The air utilization rises sharply when the power demand increases, while the fuel utilization suddenly drops. The reason for the spike in air utilization is the rapid increase of oxygen consumption rate in SOFC, which is caused by the increase in current density caused by higher hydrogen concentration due to the increase of fuel flow rate. On the contrary, fuel utilization drops even though the hydrogen consumption rate increases in the SOFC because the increase in fuel flow is larger than the increased hydrogen consumption rate. Both fuel and air utilization are closely related to current density and this relation can be seen in Fig. 9.

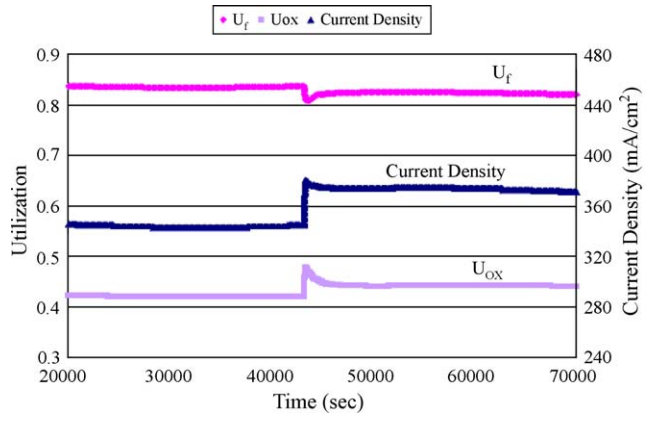

Fig. 9. Air and fuel utilization and current density. This graph shows how fuel utilization, oxygen utilization, and current density change during the same transient performance period. Fuel utilization decreases a little after the load step change, while oxidant utilization and current density increase.

Table 4
Predicted system performance without SOFC temperature control

Compressor out T (K)	423
Recuperator out T (K)	1390
Cathode out T (K)	1238
Anode out T (K)	1232
Combustor out T (K)	1711
High-pressure turbine out T (K)	1602
Power turbine out T (K)	1530
Compressor exit P (kPa)	264
Air flow rate (kg s^{-1})	0.033
U_f	066
U_{air}	0.39
Current Density (mA cm^{-2})	353
Fuel cell power output (kW)	28.2
Gas turbine power output (kW)	4.7
Total power output (kW)	32.9
Fuel	33.3% CH_4, 667% H_2O

This table shows the steady state performance of system without temperature control. Temperatures are much too high for many of the materials typically used in components such as the recuperator in this case. Methods for controlling these temperatures are necessary.

3.4. Maintaining system temperatures

In this section the importance and capability of maintaining system temperatures in the current system is investigated. Table 4 shows the temperatures of each point of the system for a simulation case wherein the fuel cell temperature controller previously implemented was not used (turned off). Note that the operating temperature of the SOFC is around 1240 K, which is adequate, but the temperature of combustor exit is over 1700 K. This high temperature cannot be tolerated either by metal or ceramic turbine blades. This high combustor exit temperature is caused by a high temperature in upper stream of the recuperator caused by the high operating temperature of the SOFC. High SOFC operating temperature causes the Nernst potential to drop. Since the SOFC is maintained at a voltage of 0.7 V, current density drops, leading to a drop in fuel utilization. As fuel utilization drops, more fuel goes to the combustor, creating an even higher combustor exit temperature, eventually increasing the power turbine exit temperature. This high temperature gas leaving power turbine exchanges more heat in the recuperator, which finally raises the temperature of the cathode inlet air stream. This self-exciting thermal process is supported by observation of the fuel utilization and current density presented in Table 4. Comparing the performance of Table 4 to that of the design point performance shown in Table 2, note that both fuel utilization and current density are lower for this case without temperature control (Table 4). This case demonstrates the importance of temperature control so that one can avoid damage to turbine blades, the recuperator, and/or the fuel cell.

One effective way to control system temperatures is to introduce a bypass flow of some amount of exhaust around the recuperator that preheats the inlet air to the SOFC. In that way, the system can avoid this type of self-exciting temperature rise by controlling the temperature of air going into the SOFC. The amount of gas bypassing the recuperator can be controlled by

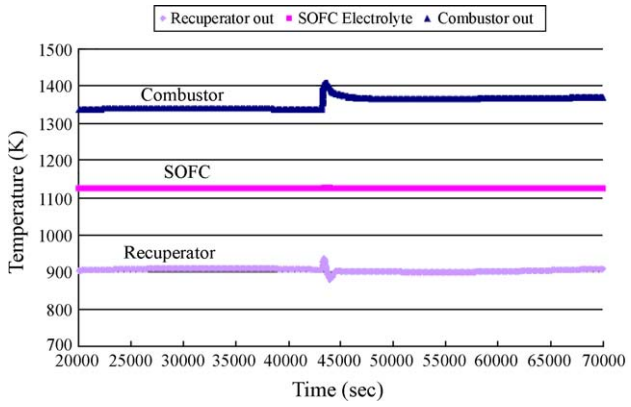

Fig. 10. Temperature variation with control strategy. This figure shows how the temperatures throughout the hybrid system are controlled while operating on a fluctuating biomass gas and while, power demand is changed in step-wise fashion at a time of 43,000 s. The SOFC stack temperature is kept constant by the controller connected to the bypass valve. There remains a steep jump in combustor outlet temperature for a short period during the load demand change, but this is significantly lower than the uncontrolled case.

a valve, which position is changed based on the temperature of the SOFC.

Fig. 10 shows the temperature transient of the system in response to the step change of power demand with the newly introduced manipulation of recuperator bypass. The fuel used here is the same biomass gas fuel used in Section 3.2. Fig. 10 shows that the combustor exit temperature is 1410 K at most, which is nearly 300 K lower than the non-controlled case presented in Table 4. The performance of the system with power and temperature control is shown in Table 5. The SOFC temperature is effectively maintained at 1123 K, or 850 °C in this case, through use of the recuperator bypass control. Note that the combustor exit temperature is still high for a traditional micro turbine blade, although 1410 K could be endured by a ceramic turbine. Temperature is not expected to reach such high levels in the experimental system due to heat losses. Since details of the particular integrated hybrid design are not known and since this was not the focus of the current study, these additional heat losses were not estimated.

Table 5
System performance with temperature control

Compressor out T (K)	397
Recuperator out T (K)	907
Cathode out T (K)	1122
Anode out T (K)	1120
Combustor out T (K)	1367
High-pressure turbine out T (K)	1304
Power turbine out T (K)	1209
Compressor exit P (kPa)	221
Air flow rate (kg s^{-1})	0.036
U_f	0.83
U_{air}	0.44
Current density (mA cm^{-2})	372
Fuel cell power output (kW)	297
Gas turbine power output (kW)	53
Total power output (kW)	35
Fuel	Biomass gas

This table shows the time-averaged steady-state performance of the system with power and temperature control implemented.

Fig. 10 also shows the transient change of temperatures in the system. Note the nearly instant rise in temperature of the combustor exit when the power demand changes. This is because the combustor has a small thermal mass leading to a very small delay in temperature rise due to burning of increased unspent fuel from the SOFC. In the moment of a step change in power demand, more fuel is supplied to the SOFC to follow the change. The SOFC only consumes some amount of this increased fuel flow rate due to the fact that fuel is present in the anode compartment sufficient to meet the previous lower demand of previous times. This makes anode off-gas of the SOFC richer in fuel and leads to higher temperature in the combustor with no delay. In addition, Fig. 10 shows a slower temperature decrease after the initial jump. This is caused by higher combustor exit temperatures that lead to increases in high-pressure turbine power. This drives the compressor to produce more mass flow of air, eventually lowering combustor exit temperature by diluting the combusted gas.

Fig. 11 shows the change of the recuperator efficiency and the gas portion that goes through the lower stream (turbine exhaust) of the recuperator. The valve starts to provide a new value when the power demand is changed because the system temperatures begin to change at that moment.

The recuperator efficiency remains at approximately 88%. During the transient response, however, it leaps up and drops down for a time between 82 and 95%. This is because the valve starts to release more exhaust gas to the environment, bypassing the recuperator. At the moment of the step change, the bypass valve releases more exhaust gas to the environment and the flow rate of gas going into the recuperator decreases. Decreased flow rate of exhaust gas produces longer residence time in the recuperator and exchanges more heat, leading temporarily to the higher observed efficiency of the recuperator. Note that recuperator efficiencies are relatively high in the current case due to a very large recuperator surface area. Note that slow and small

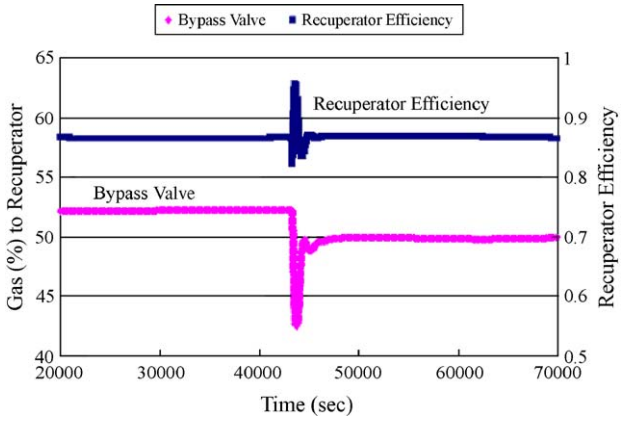

Fig. 11. Recuperator bypass valve variation. This figure shows how recuperator efficiency changes as the system with all controllers implemented responds to the step change in load. The amount of gas going into the recuperator decreases after the change to avoid overheating. Even though a varying amount of gas goes into the recuperator, the efficiency remains about the same.

changes are observed after reaching to the new steady state due to the biomass fuel fluctuation.

4. Conclusions

Power and temperature control of a fluctuating biomass fueled small sized SOFC-MGT hybrid system is developed based on dynamic modeling of the integrated hybrid system. The designed performance of the system is to produce 35 kW with the contribution of SOFC and MGT power set at 85 and 15%, respectively. The system efficiency at the design point operating on methane is 56.3%, which is remarkably high considering the size of the plant.

A fluctuating power output is observed when the system is fueled with biomass gases that have a fluctuating composition. Since SOFC performance is very sensitive to hydrogen concentration in the anode compartment, power output from SOFC tracks the fuel composition changes with relatively high amplitude power fluctuations. Fluctuating power output due to the fuel composition fluctuations can also be seen from the MGT. However, the fluctuating MGT power amplitude is smaller than that of the SOFC. This is because the MGT runs only on the waste heat and spent fuel of SOFC that do not fluctuate as much with changes in biomass fuel gas composition.

Two controllers are developed and implemented in the dynamic model to control power and fuel cell temperature in response to a step change in power demand. The first controller controls power output by manipulating the flow rate of biomass gas. The MGT passively and rapidly responds to contribute to total system power as the SOFC power responds with a longer transient response time. The fuel controller successfully controlled the system for a step change in power demand from 32 to 35 kW, maintained system power output at 35 kW even with fluctuating fuel composition. The second controller was developed to control the temperature of the SOFC by introducing and manipulating a bypass valve around the recuperator. By bypassing some turbine exhaust flow to the environment, in the controller successfully maintained SOFC temperature at 850 °C, and reduced the combustor exit temperature to an acceptable level of 1400 K.

Acknowledgements

This research was carried out within the graduate exchange program between University of California, Irvine and University of Tokyo, Japan. The authors would like to express their thanks to R. Roberts and F. Mueller for their kind assistance.

References

[1] R. Yinger, Behavior of Capstone and Honeywell Microturbine Generators during Load Changes, Southern California Edison, July 2001.
[2] Energy white paper, Ministry of Economy, Trade and Industry of Japan, 2004 (Japanese).
[3] Fuel Cell Handbook. U.S. Department of Energy, Office of Fossil Energy, National Energy Technology Laboratory, November 2002.
[4] J. Palsson, A. Selimovic, L. Sjunnesson, Combined solid oxide fuel cell and gas turbine systems for efficient power and heat generation, J. Power Sources 86 (2000) 442–448.
[5] S.H. Chan, H.K. Ho, Y. Tian, Multi-level modeling of SOFC-gas turbine hybrid system, Int. J. Hydrogen Energy 28 (2003) 889–900.
[6] P. Kuchonthara, S. Bhattacharya, A. Tsutsumi, Energy recuperation in solid oxide fuel cell (SOFC) and gas turbine (GT) combined system, J. Power Sources 117 (2003) 7–13.
[7] P. Costamagna, L. Magistri, A.F. Massardo, Design and part-load performance of hybrid system based on a solid oxide fuel cell reactor and a micro gas turbine, J. Power Source 96 (2001) 352–368.
[8] L. Magistri, P. Costamagna, A.F. Massardo, C. Rodgers, C.F. McDonald, A hybrid system based on a personal turbine (5 kW) and a solid oxide fuel cell stack: a flexible and high efficiency energy concept for the distributed power market, J. Eng. Gas Turbines Power 124 (2002) 850–857.
[9] S.H. Chan, H.K. Ho, Y. Tian, Modeling for part-load operation of solid oxide fuel cell-gas turbine hybrid power plant, J. Power Source 114 (2003) 213–227.
[10] R.S. Gemmen, E. Liese, J.G. Rivera, F. Jabbari, J. Brouwer, Development of Dynamic Modeling Tools for Solid Oxide and Molten Carbonate Fuel Cell Gas Turbine Systems, International Gas Turbine Institute meeting of ASME, May 2000.
[11] R.A. Roberts, F. Jabbari, J. Brouwer, R.S. Gemmen, E.A. Liese, Inter-Laboratory Dynamic Modeling of a Carbonate Fuel Cell For Hybrid Application, ASME Turbo Expo 2003, June 2003.
[12] R.A. Roberts, J. Brouwer, E. Liese, R.S. Gemmen, Dynamic Simulation of Carbonate Fuel Cell-Gas Turbine Hybrid Systems, ASME Turbo Expo 2004, June 2004.
[13] L. Magistri, M.L. Ferrari, A. Traverso, P. Costamagna, A.F. Massardo, Transient Analysis of Solid Oxide Fuel Cell Hybrids Part C: Whole Cycle Model, ASME Turbo Expo 2004, June 2004.
[14] M.A. Khaleel, Z. Lin, P. Singh, W. Surdoval, D. Collin, A finite element analysis modeling tool for solid oxide fuel cell development: coupled electrochemistry, thermal and flow analysis in MARC, J. Power Sources 130 (2004) 136–148.
[15] J. Xu, G.F. Froment, Methane steam reforming, methanation and water-gas shift: I. Intrinsic kinetics, AIChE J. 35 (1989) 88–96.
[16] J. Xu, G.F. Froment, Methane steam reforming: II. Diffusional limitations and reactor simulation, AIChE J. 35 (1989) 97–103.